

## Evidence of microbial activity involved with Neoproterozoic postglacial sediments from the Otavi Group, Namibia: a study of Sturtian oolitic carbonate sandstone with spectroscopic methods

Ildikó Gyollai<sup>2</sup>, Márta Polgári<sup>2</sup>, Miklós Veres<sup>3</sup>, Szabolcs Nagy<sup>4</sup>, Friedrich Popp<sup>5</sup>, Dieter Mader<sup>1</sup>, Christian Koeberl<sup>1,6</sup>

<sup>1</sup>Department of Lithospheric Research, University of Vienna, Althanstrasse 14, A-1090, Vienna, Austria;

<sup>2</sup>Research Centre for Astronomy and Geosciences, Geobiomineralization and Astrobiological Research Group Institute for Geology and Geochemistry, Hungarian Academy of Sciences, 1112 Budapest, Budaiörsti út. 45, Hungary;

<sup>3</sup>Research Institute for Solid State Physics and Optics of Hungarian Academy of Sciences, Budapest, Hungary; <sup>4</sup>Department of Mineralogy, Geochemistry and Petrology, Szeged University, 6702 Szeged, Egyetem utca 2-6, Hungary;

<sup>5</sup>Department of Geodynamics and Sedimentology, University of Vienna, Althanstrasse 14, A-1090, Vienna, Austria;

<sup>6</sup>Natural History Museum, Vienna, A-1010, Burgring 7, Vienna, Austria

Corresponding author: Márta Polgári, e-mail: rodokrozit@gmail.com

**Abstract:** Basal layers from Sturtian postglacial cap carbonate deposits of the Otavi Group, Namibia were studied using various spectroscopic methods in order to define their paleoenvironmental sedimentary conditions, as well as their presumptive micro-fossil record. Deposition of our sample set occurred in shallow water environments during the aftermath of the Sturtian „Snowball Earth” glaciation. Onion-like growth structures related to ironoxidizing bacteria and cyanobacteria were observed randomly in the interior of ooids and also within micritic matrix material. The Raman spectroscopic detection of various hydrocarbon phases contained in our samples strongly point to bacterial activity involved with sediments allocated to the immediate aftermath of Sturtian „Snowball Earth” glaciations. Backscattered electron imaging and cathodoluminescence microscopy of fine-grained detrital matrix material illustrate a variety of minerals, such as zircon, mica, feldspar, and apatite, all of which indicate detrital input derived from crystalline basement areas. Smectite around the ooids was most probably generated by diagenesis of iron-oxidizing bacterial films.

**KEYWORDS:** Sturtian glaciation, Neoproterozoic, ooid, oncolite, micro-Raman, cathodoluminescence, microbial record, cyanobacteria, iron-oxidizing bacteria, paleoenvironmental reconstruction

### Introduction

#### Overview

Observational evidence suggests that Planet Earth went through several episodes of global or near-global glaciations during the Late Precambrian Period (Hoffman and Schrag, 2002). The so-called “Snowball Earth” hypothesis states that the Sturtian (~750 Ma) and Marinoan (~635 Ma) glaciations were of global extent and may have lasted for several million years (Hoffman et al., 1998). A variation of this hypothesis, called the “Slushball Earth”, assumes intermediate conditions without substantial equatorial sea ice (Harland and Rudwick, 1964). While the “Snowball Earth glaciations”

would have ended abruptly in a greenhouse environment, the “Slushball Earth glaciations” ought to be characterized by a slower, gradual deglaciation process (Fairchild and Kennedy, 2007). Concerning the initiation of a global glaciation process a variety of causes have been discussed, including decreased solar luminosity, continental breakup tectonics and the passage of the Solar System through an interstellar cloud (Hoffmann and Schrag, 2002). At this stage, not only the probable cause of the glaciations is unclear, but also the cause and mechanism of deglaciation processes is debated. According to the so-called “Zipper-rift model” (Eyles and Januszczak, 2004) diachronous rifting of the former superconti-

ment “Rodinia” might have led to a global glaciation, suggesting that some part of the specific diamictites have been formed from turbidity currents. However, our study confirms the existence of distinct ancient areas characterized by specific environmental conditions attended by the Sturtian deglaciation process. Our discovery of fossilized microbial textures is the focus of this study, which attempts to provide evidence of organic material incorporated within these putative microbial remains.

### Geological background

Our research area is located in the Neoproterozoic Otavi Group of NW-Namibia. The Otavi Platform formed along the southern fringe of the Congo Craton and

abuts on the continental slope facies further South and West (Fig. 1). Thus, the predominantly calcareous sedimentary successions of the unified Otavi Group were generated in a foreland position relative to the areas of the later Kaoko Belt in the West and to the Damara Belt in the South (Hoffman, 2005). The Otavi Group is subdivided into three subgroups, which are separated from each other by two glaciogenic diamictite units, the lower Chuos Formation and the upper Ghaub Formation (Hoffman, 2005; Hoffmann and Schrag, 2002). The cap carbonates succeeding these subunits might have been generated due to CO<sub>2</sub> oversaturation of the sea-water (Le Hir et al., 2008; Kennedy et al., 2008) added by the input of methane outgassing from clathrates (Kennedy et al., 2008).

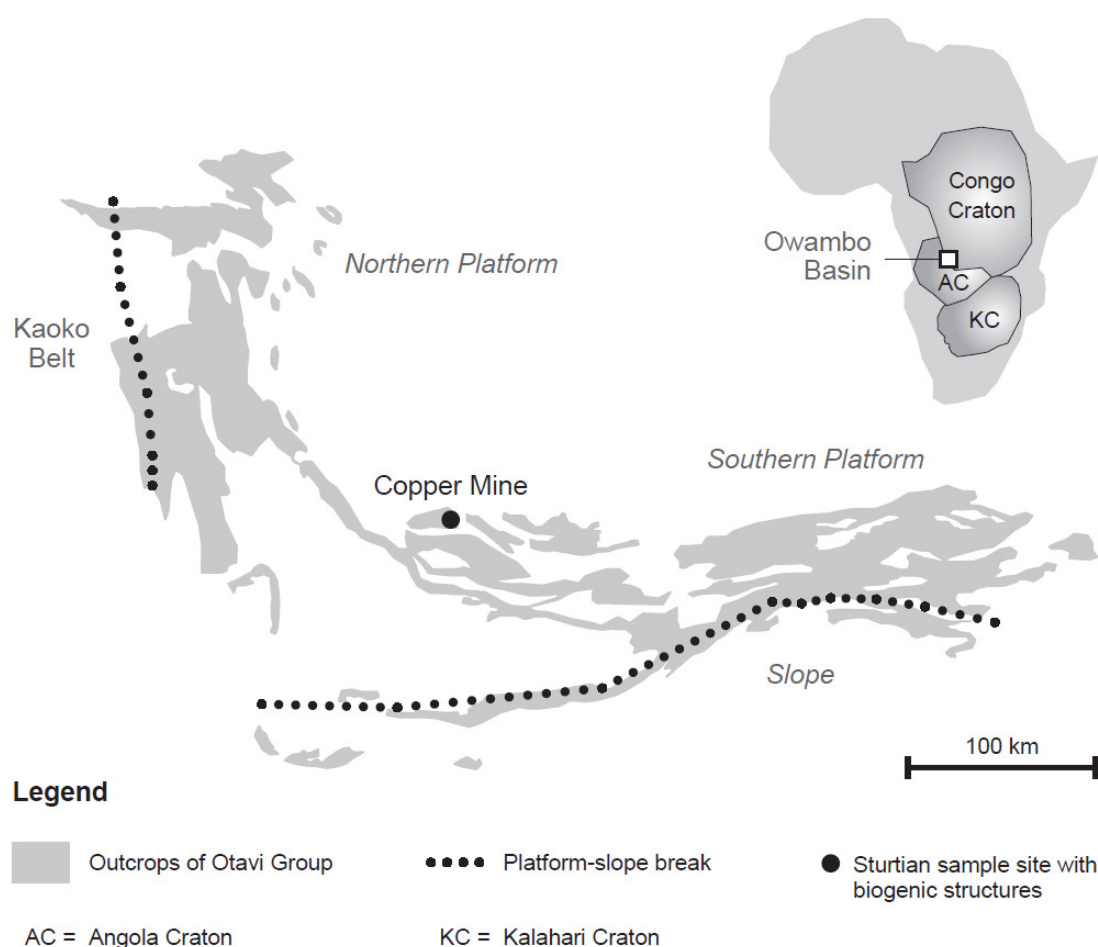


**Figure 1:** Geological map of the research area showing sampling site (Copper Mine; 9°25'18.43"S; 15° 9'50.90"E)(Modified after Hoffman, 2005).

## Samples and methods

One representative oolitic carbonate sandstone sample (C8=basal layer of the Rasthof Fm.), collected from a distinct Otavi platform facies area was studied at the Copper Mine locality (19°25'18.43"S; 15°9'50.90"E) in NW-Namibia. Macroscopic features show reddish brown- pale red color, grainstone texture with spherical carbonate components, and small quartz pebbles (Fig.

2A). Four ooid components were measured by micro-Raman spectroscopy in order to identify organic material incorporated within observed microbial structures. Pictured in Fig. 2B is a thin section of our Sturtian oolitic grainstone sample that shows the measured points. The first two investigated components were single cored ooids (oid No. 1 and 2), while the rest have multiple cores (oid No. 3 and 4).

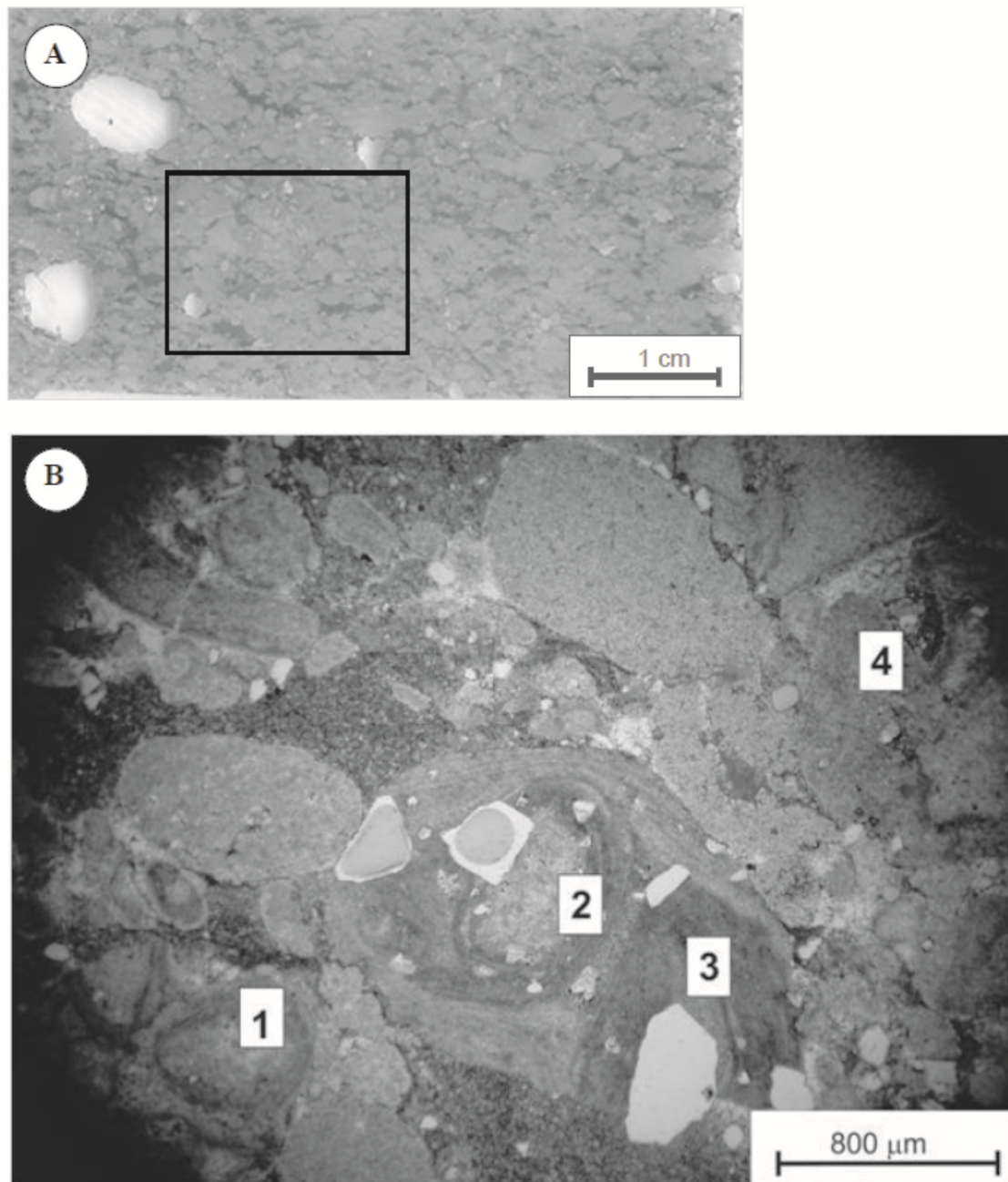


**Figure 2:** Sturtian oolitic grainstone sample. (A) photo of polished section (area of Raman measuring area – picture B is marked by black rectangle), (B) Raman measuring points signed on thin section ("ooids No. 1, 2, 3, 4"; optical microscopic photo, plain polarized light).

Scanning electron microscopy (SEM) studies were done on a polished thick section of the oolitic sandstone at the Department for Petrology and Geochemistry, Eötvös University, Budapest, Hungary. Chemical and mineral composition and distribution were determined by an Amray 1830 SEM with an EDAX PV9800 energy dispersive spectrometer detector, using 20 kW accelerating voltage, a beam current of 1nA with a defocused spot size of 10–50 nm and a collection time of 100 s.

The mineral assemblages and textures were also characterized by a NIKON ECLIPSE LV100POL optical microscope at University of Vienna and by a NIKON ECLIPSE 600 at the Institute for Geology and Geochemistry, RCAG, Hungarian Academy of Sciences, Budapest.

Raman spectra were recorded with a Renishaw Rm-2000 Raman spectrometer attached to a Leica DM/LM microscope (785 nm, 8mW laser line) at the Research Institute for Solid State Physics and Optics, Budapest.

Optical cathodoluminescence microscopy on a carbon coated polished thin section was performed with a Lumic HC5-LM system at the Department of Lithospheric Research, University of Vienna, using a beam energy of 14 keV and a beam current of ~0.20 mA. Image acquisitions were done with a KAPPA DX 40 C camera system.

## **Results**

### **Petrography**

The studied basal cap carbonate sample (C8) is an oolitic "wackestone" to "packstone" with respect to Dunham's classification on dominant texture (Dunham, 1962) which formed at winnowed inner platform facies (Fig. 2). Some ooid grains are wrapped with micritic rims generating oncoid sedimentary structures. These oncoids can include one or more cores of different mineralogical composition. In cases of single cored oncoids the composition is micritic,

similarly to the matrix of the oncoid. If the oncoids are multicored their composition consists of detrital minerals, like quartz and mica. Recrystallized quartz lenses also occur among the oncoid's cores. The micritic matrix contains mica, quartz, and carbonate. A few clasts are bordered/framed with fibrous mica. Quartz grains coated by sericite indicate very low grade metamorphic reactions. Based on microtexture, the dark micritic rims surrounding cores of dolomitic oncoids are assumed to be of bacterial origin (Fig. 2).

### **Microbial structures**

Signs of Fe-oxidizing bacterial activity (FeOB) were observed in sample C8 located at the filamentous rims of the ooids and their onion-shape like internal structures (Fig. 3). Some supposable coccoidal iron oxidizing bacteria (FeOB) colonies are located perpendicularly to the growth rims of the ooids, being indicative of septum structures. These phenomena indicate that the putative FeOB colonies expanded upon ooid surfaces, and were repeatedly buried by following generations of carbonate films created by metabolism of calcimicrobae and cyanobacteria (Fig 4). Growth sequences of the observed FeOB colonies start randomly onto micritic carbonate nuclei then advancing towards their inner part. Compared to these carbonate nuclei quartz grains often offer a better preservation of this aspect (Fig. 4). Our samples exhibit mainly coccoidal colonies of FeOB. In general, the observed FeO colonies apparently developed in symbiosis of cyanobacteria and calcimicrobae with diatom-like microorganisms characterized by similar shape and SiO<sub>2</sub>-bearing frustules incorporated in quartz.

### **Chemical composition and mineralogy - backscattered electron imaging**

The bulk mineral composition of C8 oolitic packstone is 84 wt.% carbonate, 15 wt.% mica, 5 wt.% quartz and K-feldspar, and 1 wt.% hematite, as determined by optical microscopy.

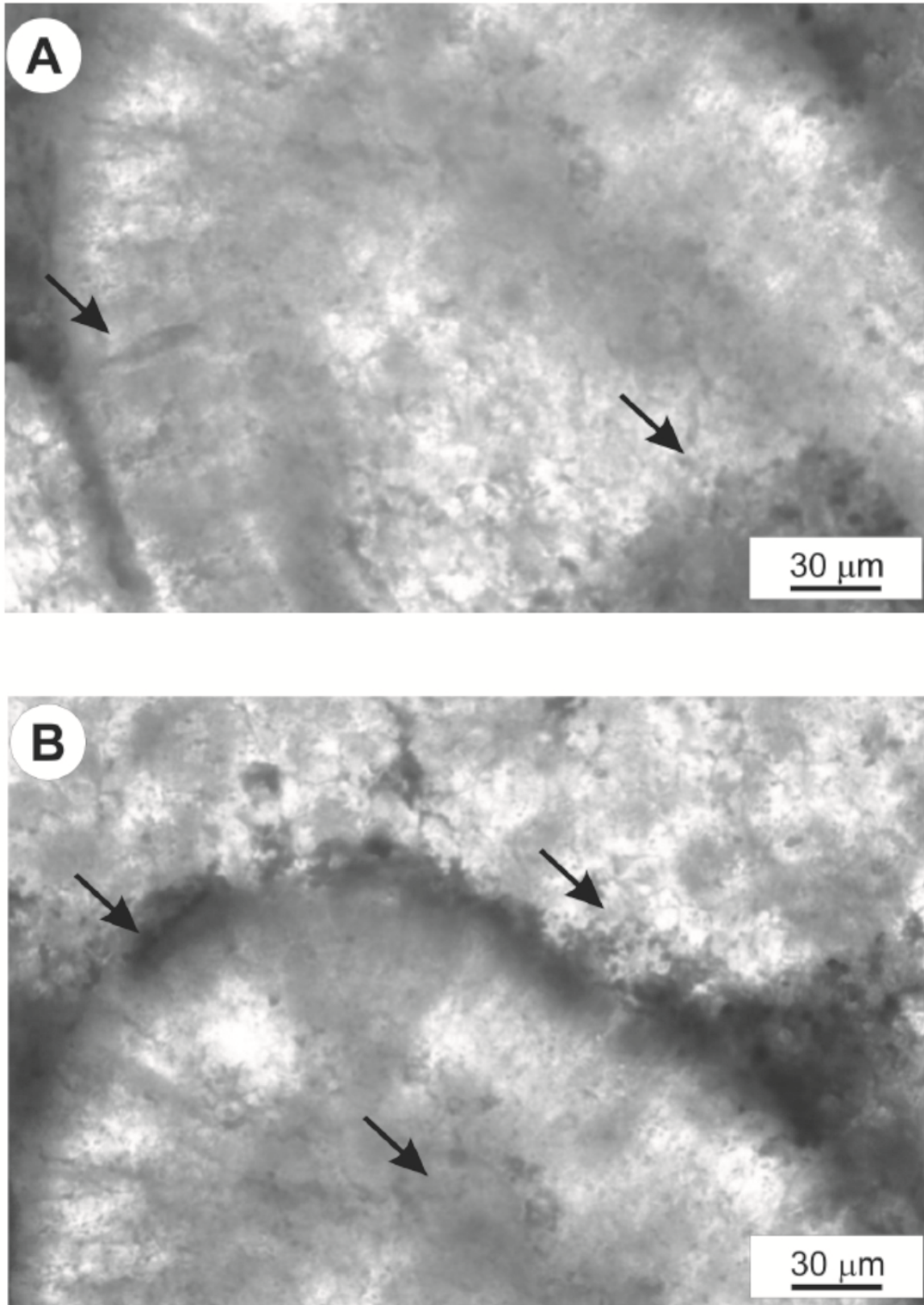


**Figure 3:** FeOB colonies on the surface of ooids and inside along of growth of ooids (in symbiosis with cyanobacteria and calcimicrobae (shown by arrows). (A) FeOB colonies perpendicularly growth inside ooids, (B) FeOB colonies on surface of ooid.

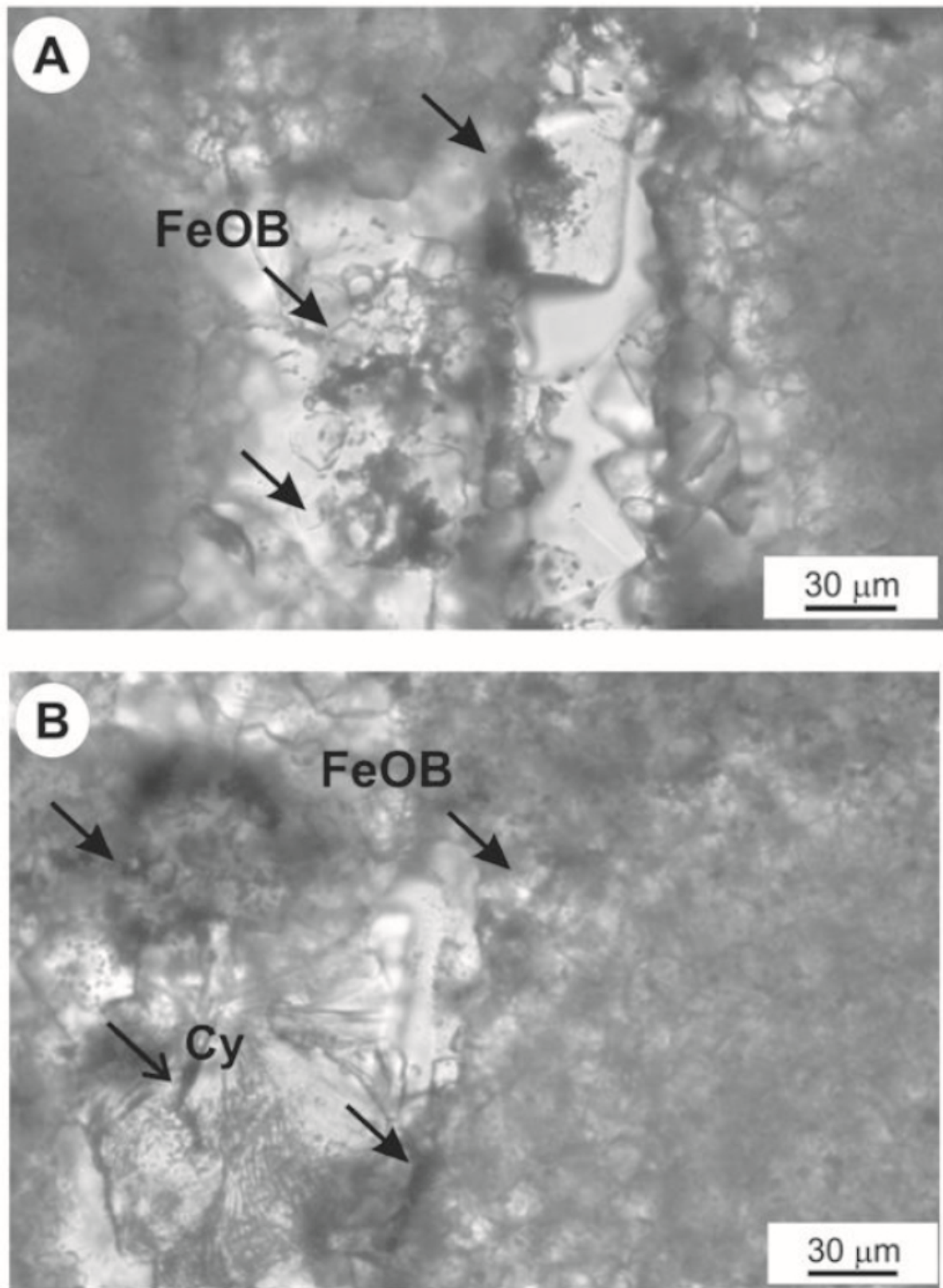


**Figure 4:** FeOB colonies on the surface of quartz pebbles (A) and in symbiosis with oscillatory cyanobacteria (Cy) (B) (shown by arrows).

The analyzed ooids No. 1 and 2 have a single dolomite-core, the multi-cored ooid No. 3 consists of dolomite and microcline, and ooid No. 4 has a core of dolomite and quartz. According to SEM-EDS data and back-scattered electron (BSE) images, an analyzed 3 mm sized quartz of the oolitic

packstone is surrounded by a rim of fine-grained kaolinite-barite-apatite mineral assemblage. This quartz grain is crossed by a diagenetic barite vein. The micritic ooids are usually surrounded by a smectite rim, which may contain galenite grains (Fig. 5).

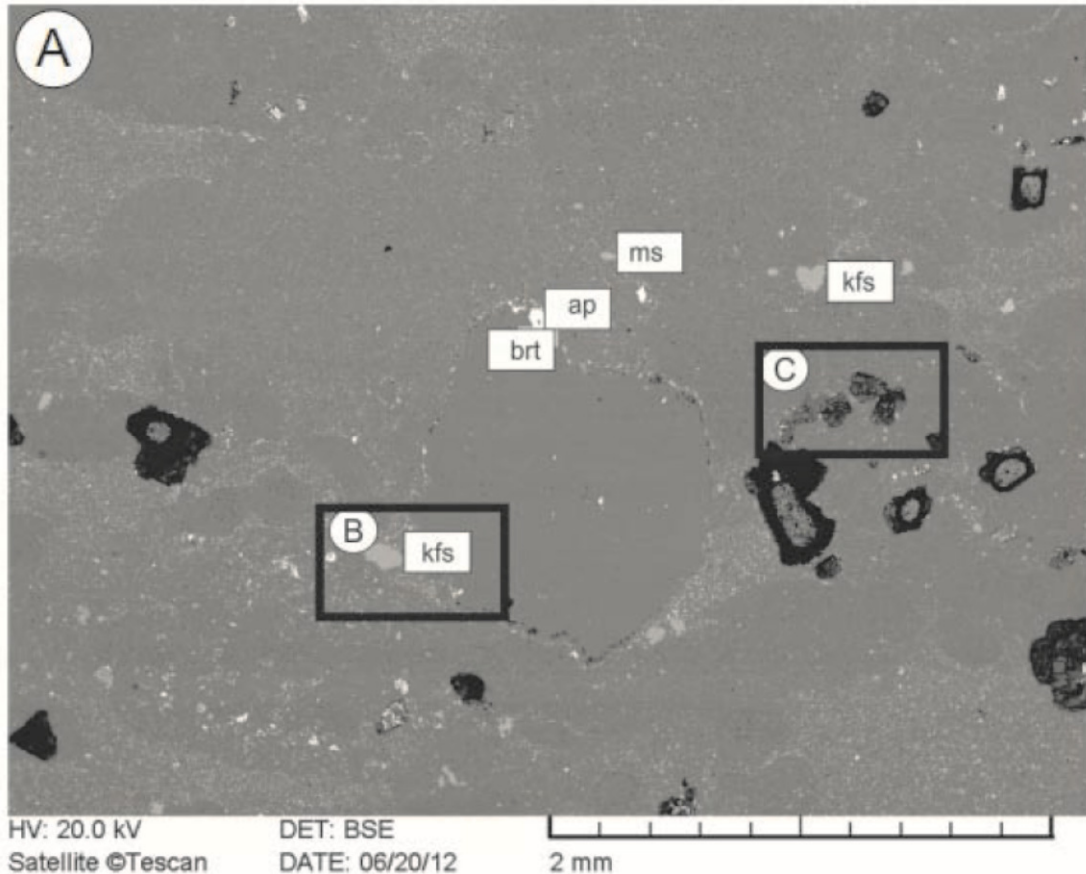


**Figure 5:** Backscattered electron image of an ooid in C8 Sturtian oolitic packstone-wackestone (A); (B) rim of quartz pebble; (C) smectite rim around ooid (Legend: brt=barite, smect= smectite, gal=galenite, kfs=K-feldspar, dol=dolomite, q=quartz, ap=apatite, ms=muscovite (B, C pictures are focused area of picture A, which are marked by black rectangle).

### ***Textural characteristics by cathodoluminescence studies***

The investigated ooid components show zoned luminescence (bright red zones in dull red material; Fig. 6). Several detrital mineral components can be observed inside the ooid structure (blue luminescent quartz and feldspar). In general, the carbonate material between oolites has a brighter red luminescent color than the oolites themselves. Bright red luminescent clasts and small grained

oolite components with bright red rim occur between larger oolite components (Fig. 7).

### ***Raman spectroscopy***

The points in our Sturtian oolitic grainstone (“ooid No. 1, 2, 3, 4”) thin section that have been measured by Raman spectroscopy are shown in Fig. 2B, and the corresponding Raman vibration data are listed in Table 1.

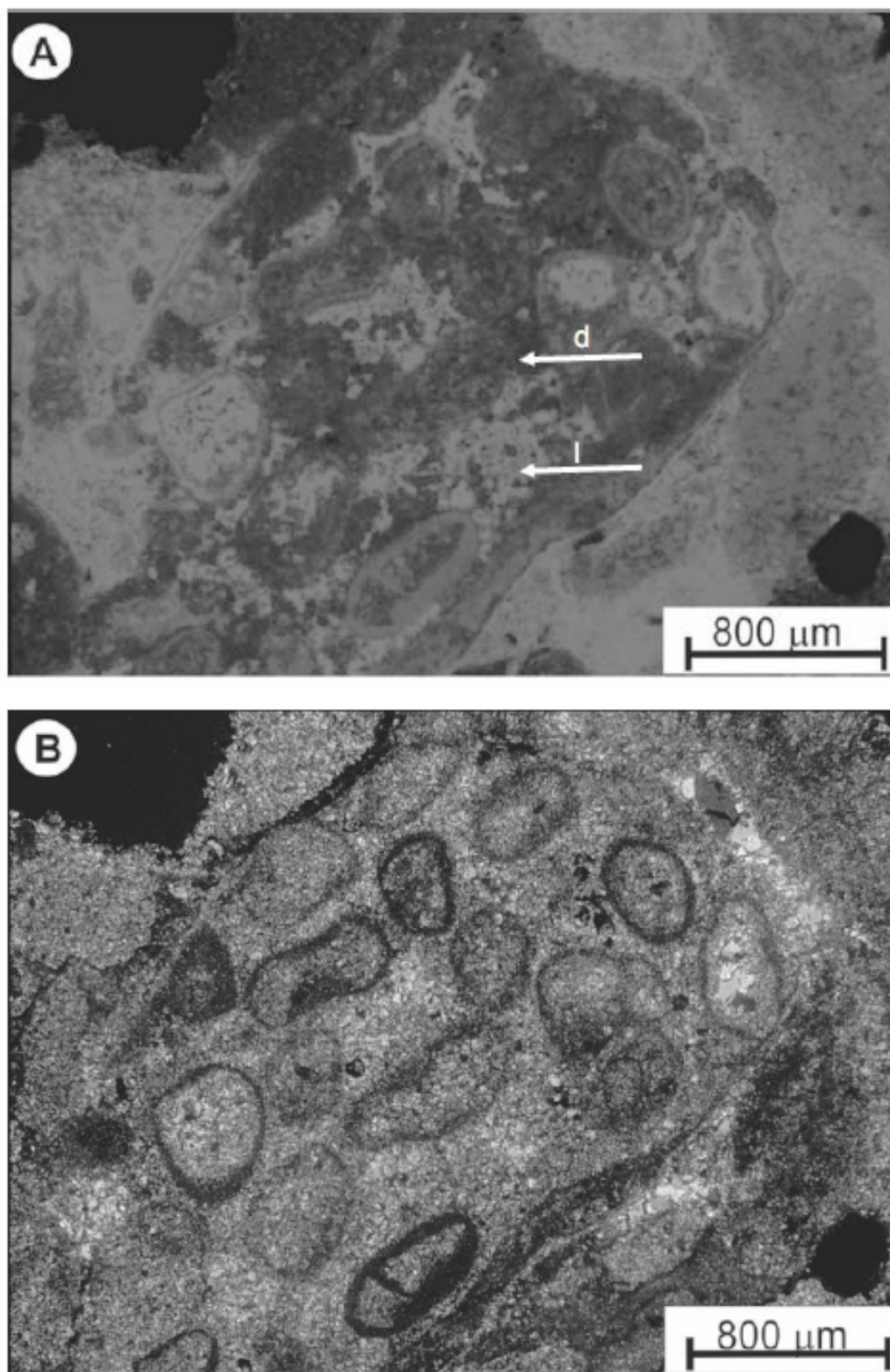


**Figure 6:** Multicore-oooid where the core is surrounded by fine-grained material (bacterial film). Inside and between the cores, light-luminescent cements are observed (l-arrow), which are filled with small grained oolite components. The dull luminescent part (d-arrow) is built up from/by clayey and carbonaceous material. (A) cathodoluminescent light, (B) plain polarized light.

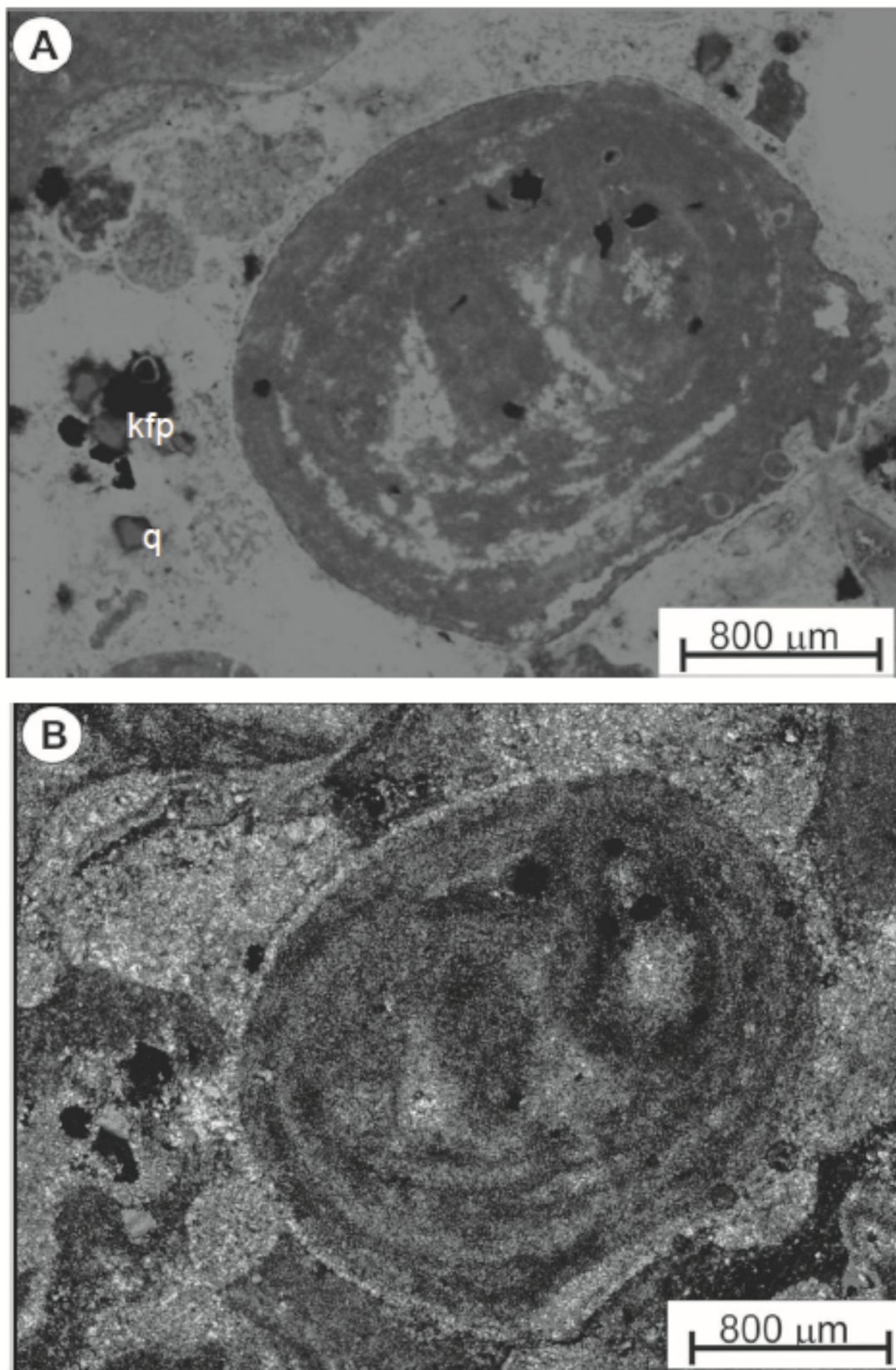


**Figure 7:** Ooids with growth rims, with brighter luminescent color. The middle luminescent grains are quartz (q) and feldspars (kfp) detrital grains (A) cathodoluminescent light, (B) plain polarized light.

Ooid No. 1:

The spectra are dominated by the narrow bands of dolomite at 178, 300, 723, and 1097  $\text{cm}^{-1}$  (Lewis and Edwards, 2001). Another remarkable feature of the spectra is the broad band in the 1000-2000  $\text{cm}^{-1}$  region, which can be attributed to  $\text{sp}^2$  C=C bonds (up to 1650  $\text{cm}^{-1}$ ) and different carbonyl and cumulated double bonds of the amorphous carbon phase with some oxygen content. Other observable peaks at 1300 and 1450  $\text{cm}^{-1}$  correspond to deformation vibrations of  $\text{CH}_2$  and  $\text{CH}_3$  groups, while the peak at 1402 belongs to asymmetric vibration of  $\text{CH}_2$  and  $\text{CH}_3$

groups. The peak of the carbonyl group can be detected at 1716  $\text{cm}^{-1}$  (Fig. 8A; Table 1A).

Ooid No. 2:

The dolomite peaks appear at 173  $\text{cm}^{-1}$ , 298  $\text{cm}^{-1}$ , 725  $\text{cm}^{-1}$  and 1099  $\text{cm}^{-1}$ , respectively. A broad band related to an amorphous carbon phase can be seen in the 1000-2000  $\text{cm}^{-1}$  region. Narrow peaks at 1302 and 1402  $\text{cm}^{-1}$  correspond to vibrations of  $\text{CH}_2$  and  $\text{CH}_3$  groups. The stretching vibration of the carbonyl group appears at 1717  $\text{cm}^{-1}$  (Fig. 8B, Table 1B).

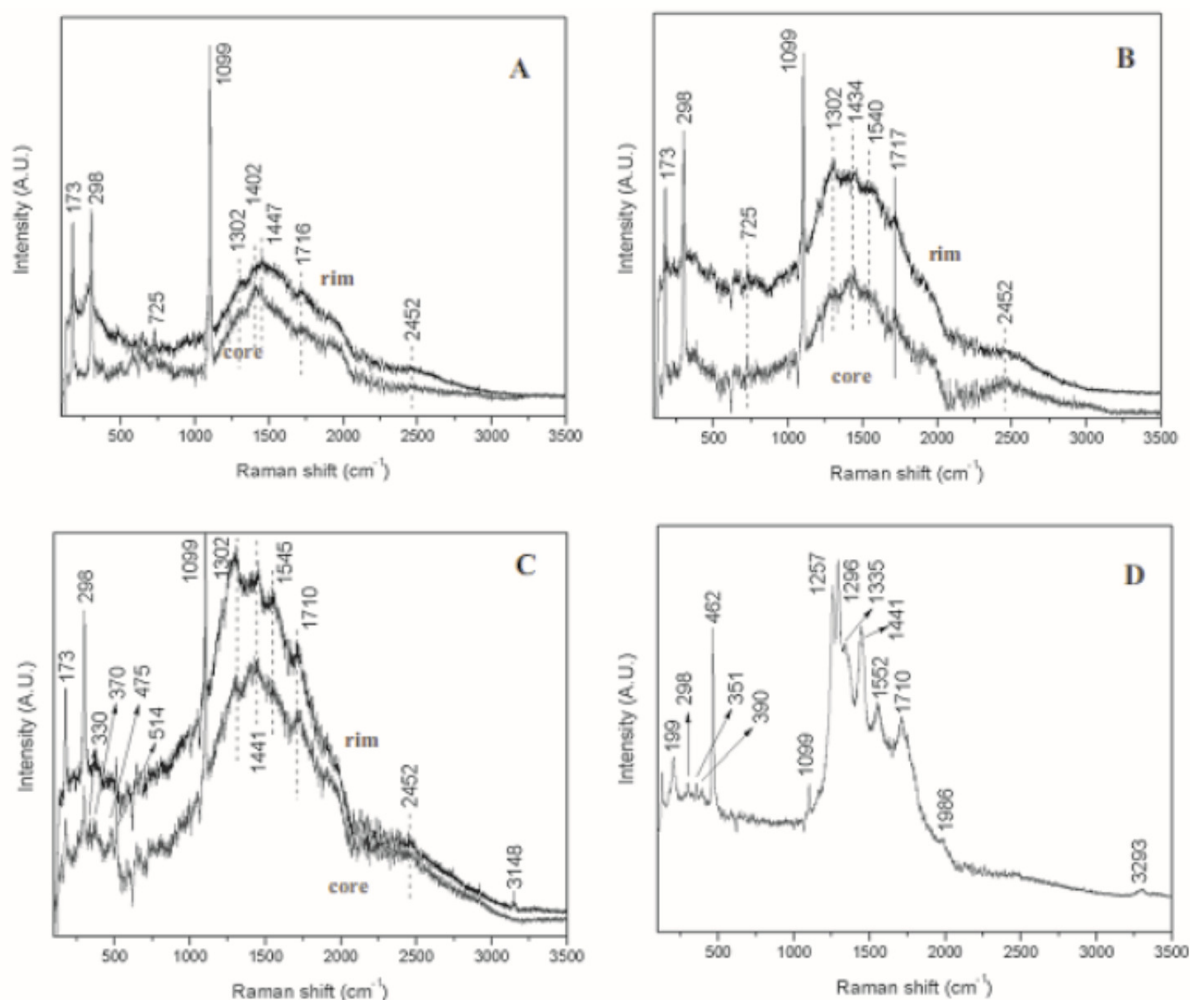


**Figure 8:** Raman spectra of ooid No. 1-4 (for measuring site see Fig. 2B, vibrations are listed in Table 1). (A) ooid No. 1, (B) ooid No. 2., (C) ooid No. 3, (D) ooid No. 4. Spectra in ooid No.1-3 were measured in core and rim region).

Ooid No. 3:

The peaks of dolomite appear at 173 cm<sup>-1</sup>, 298 cm<sup>-1</sup> and 1099 cm<sup>-1</sup>, respectively. The peak at 724 cm<sup>-1</sup> is of low intensity because of the polarization effect. The K-feldspar (microcline) shows minor peaks at 330 cm<sup>-1</sup>, 364 cm<sup>-1</sup>, and strong vibration of Si-O-Si/Si-O-Al bridges at 475 cm<sup>-1</sup>, whereas the most characteristic Raman vibration is centered at 513 cm<sup>-1</sup> concerning O symmetric motion in Si-O-Si bridges. The broad amorphous carbon band again appears in the 1000-2000 cm<sup>-1</sup> region. Some narrow CH<sub>2</sub> and CH<sub>3</sub> vibrations can be detected at 1302 and 1441 cm<sup>-1</sup>, together with the peak of C=O stretching vibration at 1710 cm<sup>-1</sup> (Fig. 8C, Table 1C).

Ooid No. 4:

The peaks of dolomite appear at 299 cm<sup>-1</sup> and 1099 cm<sup>-1</sup>. The peak at 178 cm<sup>-1</sup> overlaps with the band at 199 cm<sup>-1</sup>, while the one at 724 cm<sup>-1</sup> is affected by the polarization effect. The peaks of quartz appear at 199 cm<sup>-1</sup>, 351 cm<sup>-1</sup>, 390 cm<sup>-1</sup> and 462 cm<sup>-1</sup>. The vibrations of CH<sub>3</sub> and CH<sub>2</sub> groups are centered at 1296 cm<sup>-1</sup>, 1335 cm<sup>-1</sup> and 1441cm<sup>-1</sup>. The C=O stretching vibration is at 1710 cm<sup>-1</sup>, and a new peak can also be detected that can be attributed to some structural units with cumulated double or triple bonds. Amorphous carbon in the sample causes the broad band in the 1000-2000 cm<sup>-1</sup> region (Fig. 8D, Table 1D).

--

Standard of dolomite	Hydrocarbon	Ooid 1core	Ooid 1rim
178 Eg** T(Ca, Mg, CO <sub>3</sub> )		73 (Dol)	173 (Dol)
300 Eg (T(Ca, Mg, CO <sub>3</sub> )		298 (Dol)	298 (Dol)
723 Eg v4 symmetric CO <sub>3</sub> 723 EG v4 symmetric CO <sub>3</sub> Deformation		725 (Dol)	725 (Dol)
1097 Ag*** v1 symmetric C 1099 1099 Stretching	v v1 symmetric CO <sub>3</sub>	(Dol)	(Dol)
	1300 CH <sub>3</sub> -CH <sub>2</sub> transverse vibrations of H atoms	1302	1302
	1400 assym. vibrations of CH <sub>3</sub> and CH <sub>2</sub> groups	1402	
1450 Eg v3 asymmetric CO <sub>3</sub>	1450 CH <sub>2</sub> bend	1447	1447
	1710 C=O stretch	1716 1	716
	2450 graphite (minor peak)	2452	2452

**Table 1A:** Mineral and hydrocarbon phases with Raman vibrations in four ooids (1A: spectra of ooid No. 1)

Standard of dolomite RUFF Database	Hydrocarbon	Ooid 2 core	Ooid 2 rim
178 Eg T(Ca, Mg, CO <sub>3</sub> )		173 (Dol)	173 (Dol)
300 Eg T(Ca, Mg, CO <sub>3</sub> )		298 (Dol)	298 (Dol)
723 Eg v4 symmetric CO <sub>3</sub> deformation		725 (Dol)	725 (Dol)
723 Eg v4 symmetric CO <sub>3</sub> deformation		1099 (Dol)	71099 (Dol)
1097 Ag v1 symmetric CO <sub>3</sub> stretching	1300 CH <sub>3</sub> and CH <sub>2</sub> asym. vibr.	1302	1302
	1430-1450 sp <sup>2</sup> C=C CH <sub>2</sub> and CH <sub>3</sub> group	1434	1434
1440 Eg v3 asymmetric	1532 COOH, 1500-1550 sp <sup>2</sup> C	1540	1540
CO <sub>3</sub> stretching	sp <sup>2</sup> C		
	1710 C=O stretch	1717	1717
	2450 graphite (minor peak)	2452	2452

**Table 1B:** Mineral and hydrocarbon phases with Raman vibrations in four ooids (1B: spectra of ooid No. 2)

### Discussion

The Raman spectroscopy is a powerful method to identify organic material as biomarker of microbial structures. Precambrian microfossils were studied using this method by a number of research groups (Kudryavtsev et al., 2001; Kempe et al., 2005; Marshall et al., 2005). The aromatic ring deformation and symmetric breathing is attributed in the 1200-1400 cm<sup>-1</sup> range

(Mapelli et al., 1999). The peaks of organic material in Precambrian microfossils (e.g., acritarchs) occur around 1600 cm<sup>-1</sup>, and there is a group of bands at 1300-1350 cm<sup>-1</sup>, with broad peaks belonging to kerogen - aromatic (sp<sup>2</sup>) bonded C atoms joined together with peripheral sp<sup>2</sup> and sp<sup>3</sup>-bonded hydrocarbons (Kempe et al., 2005). A variety of peaks of apparent C=C aromatic stretching bands at 1600 cm<sup>-1</sup>, CH<sub>3</sub> terminal groups

(1345  $\text{cm}^{-1}$ ), C-H aliphatic stretching (3000-2700  $\text{cm}^{-1}$ ), and C=O vibration (1710  $\text{cm}^{-1}$ ) occur in the hydrocarbon phase (Marshall et al., 2005). In our samples the peak around 1710  $\text{cm}^{-1}$ , related to the carbonyl group, is observed in all the measured ooids, which is similar to the published data of Marshall et al. (2005), while the other reported Raman shifts join the region occupied by the broad band of hydrogenated amorphous carbon phases, the large width of which is caused by the highly disordered character of the sample. This is a remarkable difference compared to the published data mentioned above. In spite of this, some characteristic CH vibrations were observed in form of narrow peaks in the 1300-1450  $\text{cm}^{-1}$  region of our spectra (Fig. 8).

In general, the Raman spectrum of amorphous carbons consists of a broad band in the 1000-1800  $\text{cm}^{-1}$  region (Dresselhaus and Dresselhaus, 1982; Ferrari and Robertson, 2000; Veres et al., 2006). For visible and near-infrared excitations it is dominated by the characteristic peaks of sp<sup>2</sup> carbon atoms, since due to resonant processes the Raman scattering on these structural units is a few orders of magnitude higher than that on building blocks consisting of sp<sup>3</sup> C atoms. The broad band is resulting from superposition of scattering contributions from different structural units and can be divided into several regions. For near infrared excitation used in this study, peaks between 1100-1200  $\text{cm}^{-1}$  and 1400-1500  $\text{cm}^{-1}$  correspond to vibrations of sp<sup>2</sup> carbon chains (observed mainly in hydrogenated samples), between 1200-1350  $\text{cm}^{-1}$  – to breathing vibrations of sp<sup>2</sup> carbon rings (this is the so called D band) and above 1570  $\text{cm}^{-1}$  – to stretching vibrations of sp<sup>2</sup> carbon atoms in rings (the so called G band) (Veres et al., 2006). Features of the broad band observed in our spectra suggest that the amorphous carbon phase in the sample is dominated by sp<sup>2</sup> (hydro) carbon chains, with relatively minor (graphitic) sp<sup>2</sup> C ring content (Table 1). This is supported by the narrow peaks assigned to different vibrations of CH<sub>2</sub> and CH<sub>3</sub> groups. Components of the broad band in the >1650

$\text{cm}^{-1}$  region, together with the carbonyl peak indicate the presence of oxygen in the amorphous carbon structure.

Comparing the broad amorphous carbon bands, ooid No. 2 and 3 have quite a similar structure, with somewhat higher graphitic content compared to ooid No. 1 (indicated by the higher intensities in the D and G band regions) (Fig 8A-C, Table 1 A-C). In ooid No. 1 and 2 the narrow hydrocarbon peaks are less intense (Fig 8A-B). These peaks have the highest intensity in the spectrum of ooid No. 4, where the C=O shows also the most pronounced vibration (Fig. 8D, Table 1D).

The observed features of amorphous carbon phases are similar to those found in cryptocrystalline silica varieties with traces of Miocene hydrothermal biomineralization (Müller et al., 2009) and indicate the organic, probably microbial origin of the amorphous carbon phases identified in the sample. Apart from organic matter, mineral components (dolomite, hematite, quartz, feldspar) were also identified by Raman spectroscopy.

The first peak of dolomite (178  $\text{cm}^{-1}$ ) shifted to 5  $\text{cm}^{-1}$  wave number, and this was overlapped by the quartz band in the spectrum of ooid No. 4 (Table 1D). In ooids No. 3 and No. 4 the 723  $\text{cm}^{-1}$  peak did not appear in the spectra, which is due to a polarization effect (Fig 8C-D, Table 1C-D). Due to diagenesis and weathering the material was dolomitized and hematitized. A dolomitization process means infiltration of Mg-rich pore water, which changes original microbial carbonate (aragonite, calcite) to dolomite during the diagenesis. Hematite was probably formed by transformation of primary ferrihydrite originated via Fe-oxidizing bacterial activity (Konhauser, 1998). Alternatively, the hematite could be derived by continental weathering (iron-rich matrix) (Hoffman et al., 1998). The smectites around the ooids are derived most probably by diagenesis and/or weathering of microbial structures, whereas galenite formed in a biomineralization process (Erlich, 2010).

Dolomite	Microcline	Hydrocarbon	Ooid 3 core	Ooid 3 rim
178 Eg T(Ca, Mg, CO <sub>3</sub> )			173 (Dol)	173 (Dol)
300 Eg (T(Ca, Mg, CO <sub>3</sub> ))			298 (Dol)	298 (Dol)
	330		330 (mcl)	330 (mcl)
	364		370 (mcl)	370 (mcl)
	475 s Si-O-Si/Si-O-Al		475 (mcl)	475 (mcl)
	513 vs (A.g.)		514 (mcl)	514 (mcl)
723 Eg v4 symmetric CO <sub>3</sub> deformation				
1097 Ag v1 symmetric CO <sub>3</sub> stretching			1099 (Dol)	1099 (Dol)
		1300 asymmetric vibrations of CH <sub>3</sub> and CH <sub>2</sub> group	1302	1302
1440 Eg v3 asymmetric CO <sub>3</sub> stretching		1450 CH <sub>2</sub> bend	1441	1441
		1532-1550 COOH	1545	1545
		1710 C-O stretch	1710	1710
		2450 graphite (minor peak)	2452	2452
		2900-3300 CH stretching vibration		3148

**Table 1C:** Mineral and hydrocarbon phases with Raman vibrations in four ooids (1C: spectra of ooid No. 3)

### Conclusions

A representative sample (C8) was analyzed for its organic geochemistry and mineral composition as well as for its textural characteristics. The presence of amorphous carbon was demonstrated in all of the measured points of the sample. Traces of hydrocarbons and C=O groups were detected, featuring

highest concentrations in the dolomite-quartz matrix. Ooid 1 and 2 hold light hydrocarbon (with low C number) of the methyl group, whereas ooid 4 contains a more complex hydrocarbon, similar to butane.

We consider the hydrocarbons detected in our samples (C8) to originate from bacterial (probably cyanobacteria) communities which existed in shallow water environments

of the ancient Otavi platform. Smectite surrounding the ooid grains is most probably derived from diagenesis and/or weathering of microbial films. Numerous peaks attributed to the methyl group might indicate a

contribution from methane outgassing and thus indicate the role of rapid global warming after Neoproterozoic “Snowball Earth” glaciations.

Standard quartz (Raman) shift) in cm-1)	Standard of dolomite RUFF Database	Hydrocarbon	Ooid 4
	178 Eg T(Ca, Mg, CO <sub>3</sub> )		
203			199 (Q)
	300 Eg (T(Ca, Mg, CO <sub>3</sub> ))		298 (Dol)
353			351 (Q)
393.5			390 (Q)
461 vs			462 (Q)
	723 Eg v4 symmetric CO <sub>3</sub> deformation		
	1097 Ag v1 symmetric CO <sub>3</sub> stretching		1099 (Dol)
		1000-1275 C-O stretching	1257
		1300 asymmetric vibration of CH <sub>2</sub> -CH <sub>3</sub> group	1296
		1335 amorphous carbon	1335
		1450 CH <sub>2</sub> bend	1441
		1532-1550 COOH	1552
		C=O stretch	1710
		2000 sp <sup>2</sup> C	1986
		3300 C-H stretching of butane	3293

\* Except No. 4, all of ooid specimens were measured at rim and in core. Mineral standards were taken from RUFF database. Hydrocarbon vibrations were interpreted following Kudryavtsev et al. (2001); Kempe et al. (2005); Marshall et al. (2005); Veres et al. (2006). Raman shifts are added in cm<sup>-1</sup>. For measuring site see Fig. 2B, for spectra see Fig. 8A-D.

\*\* Eg: marks minor vibrations in Raman spectrum.

\*\*\* Ag: defines major vibration, which is most characteristic vibration for adjacent phase in Raman spectrum.

**Table 1D:** Mineral and hydrocarbon phases with Raman vibrations in four ooids (1D: spectra of ooid No. 4)

## Acknowledgements

This study was supported by the Austrian Academy of Sciences (grant number: IGCP 512). We are grateful to the Geological Survey of Namibia and especially Director Dr. G. Schneider for invaluable help in field work organization and sample export management.

## References

- Dunham, R.J., 1962: Classification of carbonate rocks according to depositional texture.- In Ham, W.E. (ed.): Classification of carbonate rocks.- Amer. Assoc. Petrol. Geol. Memoir, **1**: 108 – 121.
- Dresselhaus, M.S. and Dresselhaus, G. 1982. Light scattering in graphite intercalation compounds. *Light Scattering in Solids III, Top. App. Phys.*, **51**, 3-57.
- Erlich, H. 2010. Biominerals. In: Erlich, H. *Biological Materials of Marine Origin - Biologically-Inspired Systems*, **1**, 25-50.
- Eyles, N. and Januszczak, N. 2004. ‘Zipper-rift’: a tectonic model for Neoproterozoic glaciations during the breakup of Rodinia after 750 Ma. *Earth-Sci. Rev.*, **65**, 1-73.
- Fairchild, I.J. and Kennedy, M.J. 2007. Neoproterozoic glaciation in the Earth system. *J. Geol. Soc. London*, **164**, 895-921.
- Ferrari, A.C. and Robertson, J. 2000. Interpretation of Raman spectra of disordered and amorphous carbon. *Phys. Rev. B*, **61**, 14095–14107.
- Harland, W.B. and Rudwick, M.J.S. 1964. The great Infra-Cambrian glaciation. *Scientific American* **211**, 28-36.
- Hoffman, P.F. 2005. 28th DeBeers Alex Du Toit Memorial Lecture (2004): On Cryogenian (Neoproterozoic) ice-sheet dynamics and the limitations of the glacial sedimentary record. *S. Afr. J. Geol.*, **108**, 557-576.
- Hoffman P.F. and Schrag D.P. 2002. The Snowball Earth hypothesis: testing the limits of global change. *Terra Nova*, **14**, 129-155.
- Hoffman, P.F.; Kaufman, A.J.; Halverson, G.P. and Schrag, D.P. 1998. A Neoproterozoic snowball Earth. *Science*, **281**, 1342-1346.
- Kempe, A.; Wirth, R.; Altermann, W.; Stark, R.W.; Schopf, J.W. and Heck, W.M. 2005. Focussed ion beam preparation and in situ nanoscopic study of Precambrian acritarchs.- *Precambrian Res.*, **140**, 36–54.
- Kennedy, M.; Mrofka, D. and von der Borch, C. 2008. Snowball Earth termination by destabilization of equatorial permafrost methane clathrate. *Nature*, **453**, 642-645.
- Konhauser, K.O. 1998. Diversity of bacterial iron mineralization. *Earth-Sci. Rev.*, **43/3–4**, 91-121.
- Kudryavtsev, A.B.; Schopf, J.W.; Agresty, D.G. and Wdowiak T.J. 2001. In situ laser-Raman imagery of Precambrian microscopic fossils. *PNAS*, **98/3**, 823–826.
- Le Hir, G.; Donnadieu, Y.; Godderis, Y.; Pierrehumbert, R. T.; Halverson, G. P.; Macouin, M.; Nedelec, A.; and Ramstein, G. 2008. The snowball Earth aftermath: Exploring the limits of continental weathering processes. *Earth Planet. Sci. Lett.*, **277**, 453-463.
- Lewis, I.R. and Edwards, H. 2001. *Handbook of Raman Spectroscopy: From the Research Laboratory to the Process Line*. Taylor and Francis, 1072 pp.
- Mapelli, C.; Castiglioni, C.; Zerbi, G. and Mullen, K. 1999. Common force field for graphite and polycyclic aromatic hydrocarbons. *Phys. Rev.* **B60**, 12710–12725.
- Marshall, C.P.; Javaux, E.J.; Knoll, A.H. and Walter, A.M. 2005. Combined micro-Fourier transform infrared (FTIR) spectroscopy and micro-Raman spectroscopy of Proterozoic acritarchs: A new approach to palaeobiology. *Precambrian Res.*, **138**, 208–224.
- Müller, A.; Polgári, M.; Gucsik, A.; Nagy, Sz.; Veres, M.; Pál-Molnár, E.; Götze, J.; Cserhádi, C.; Németh, T. and Hámor-Vidó, M. 2009. Cathodoluminescent features and Raman spectroscopy of Miocene hydrothermal biomineralization embedded in cryptocrystalline silica varieties, Central Europe, Hungary. Abstract

volume, Conference on Micro Raman Spectroscopy and Luminescence Studies in the Earth and Planetary Sciences, *AIP Proceedings CP1163, Micro-Raman Spectroscopy and Luminescence Studies in the Earth and Planetary Sciences* (Gucsik A. (ed).), p. 207-218.

Veres, M.; Tóth, S. and Koós, M. 2006. New aspects of Raman scattering in carbon-based amorphous materials. *Diamond and Related Materials*, **17**, 1692-1696.